2024

Generalization of Planck's Law and Analysis of Inflection Points and Maxima

Isaac Moncada-Almendarez

Generalization of Planck's Law and Analysis of Inflection Points and Maxima

By

Isaac Moncada-Almendarez

A Thesis

Submitted to the Division of Natural Sciences
New College of Florida
in partial fulfillment of the requirements for the degree
Bachelor of Arts

Under the sponsorship of Dr. Mariana Sendova

Sarasota, Florida
April 2024

Abstract

The study proposes generalizations of 18 mathematical forms of Planck's thermal radiation law. Sixteen transcendental equations are derived and solved for calculating the positions of three characteristic points: two inflection points and a maximum. Displacement laws for each of the characteristic points (total of 52 points), in the spirit of Wien's displacement law, are proposed. The study analyzes eight unitless probability density functions (PDFs) via proposed inflection point parameters, compared to the conventional standard deviation statistical parameter. Additionally, the proposed comparative study is utilized as a framework for linking Photobiological processes and the Planck's thermal radiation law. It is proposed that 91% of the bio-photons are bound between the two inflection points of the per-wavelength photon radiance PDF, expressed as a function of the photon energy. Finally, the study suggests extensions of the generalization of Planck's thermal radiation law to the realm of solid-state phonons.

Contents

Introduction

Central to this thesis is Planck's thermal radiation law, which can be derived from Bose-Einstein statistics [1]. More specifically the Bose-Einstein Distribution,

$$\bar{n}_{BE} = \frac{1}{e^{(\epsilon-\mu)/k_B T} - 1}. \tag{I.1}$$

Where ϵ is the energy of each particle (hf for photons), μ is the chemical potential (zero for photons), k_B is the Boltzmann constant, and $\bar{n}_{BE}$ is the number of particles in each energy state. By substituting zero for the chemical potential and hv for the energy, Eq. (I.1) returns the Planck distribution,

$$\bar{n}_{Pl} = \frac{1}{e^{hv/k_B T} - 1}. \tag{I.2}$$

The Planck distribution quantifies the number of photons in each state within a system. If we consider this system to be a one-dimensional box then the allowed wavelengths for photons are, $\lambda = 2L/n$, and allowed momentums $p = hn/2L$, where L is the length of the box and n is a positive integer [1]. The energy of a photon can be expressed in terms of momentum as $\epsilon = pc = hcn/2L$. In three dimensions n can be considered the magnitude of vector $\boldsymbol{n} = \sqrt{n_x^2 + n_y^2 + n_z^2}$. The average energy of a system is given by multiplying $\bar{n}_{Pl}$ by the ϵ and summing over $n_x, n_y,$ and n_z. The energy of the system is then given by

$$U = 2\sum_{n_x}\sum_{n_y}\sum_{n_z} \epsilon \bar{n}_{Pl} = \sum_{n_x,n_y,n_z} \frac{hcn}{L} \frac{1}{e^{\frac{hcn}{2Lk_B T}} - 1} \tag{I.3}$$

The factor of 2 accounts for waves were pairs of photons with independent polarizations. For a continuous spectrum the sums are turned into integrals resulting in Eq. (I.4).

$$U = \int_0^\infty dn \int_0^{\pi/2} d\theta \int_0^{\pi/2} d\phi \, n^2 sin\theta \, \frac{hcn}{L} \frac{1}{e^{\frac{hcn}{2Lk_B T}} - 1} \tag{I.4}$$

Evaluating the angular integrals and applying a change of variable, $\epsilon = \frac{hcn}{2L}$ and $d\epsilon = \frac{hc}{2L} dn$, then dividing by $L^3 = V$ results in Planck's thermal radiation law per energy increment.

$$\frac{U}{V} = \int_0^\infty \frac{8\pi\epsilon^3}{(hc)^3} \frac{1}{e^{\frac{\epsilon}{k_B T}} - 1} \, d\epsilon \tag{I.5}$$

$$u(\epsilon) = \frac{8\pi\epsilon^3}{(hc)^3}\frac{1}{e^{\frac{\epsilon}{k_B T}} - 1} \tag{I.6}$$

By applying a change of variable $v = \epsilon/h$ and Eq. (I.6), Planck's thermal radiation law per frequency increment can be derived. Having derived Planck's thermal radiation law per frequency increment, generalization can now begin.

Planck's thermal radiation law is traditionally presented via two probability density functions (PDFs): (i) radiance per frequency increment L_v, or (ii) radiance per wavelength increment L_λ. However, the radiance can be expressed in terms of other spectral variables, such as radiance per wavenumber increment L_k, and be expressed in either photon density rate or the radiant power density per unit area. Furthermore, each PDF can be expressed in terms of each spectral variable. Despite these functions representing the same physical law, they have distinct analytical forms. This paper proposes that generalization and subsequent analysis of the various forms of Planck's thermal radiation law, and of inflection point and peak positions, provides possible applications or extensions into the fields of Photobiology and solid-state phonon heat capacity. Furthermore, the paper suggests that generalization can be used to yield constants for various displacement laws for the different analytical forms of the thermal radiation law. The displacement laws utilize the (i) peak position to identify the value of the spectral variable for peak radiance, and (ii) the position of the inflection points to identify the proposed location of one IP standard deviation from the peak. Proposal of displacement laws is motivated by the well-known Wien's displacement law. Overall, this paper aims to: (i) generalize the thermal radiation law, (ii) propose displacement laws, (iii) suggest applications to Photobiology, and (iv) suggest an extension into solid state phonon energy and heat capacity.

Chapter 1

Thermal Radiation Law

First, I will discuss various mathematical forms of Planck's thermal radiation law (blackbody radiation) . From the spectral energy density, $u(v)dv$ of a blackbody two types of probability density functions (PDFs) will be derived. The first is the photon number density, $L^{ph}(x)$ and the second the radiation power density, $L^{W}(x)$. The PDFs will be formulated in terms of three spectral variables: frequency (v), wavelength (λ), and wavenumber (k). Finally, both PDFs for each spectral variable will be expressed in terms of the other variables for further analysis.

1.1 Spectral energy density of a black body as derived by Planck

The idea that a quantum of minimum energy cannot itself be subdivided was used by Max Planck [2] , later called photon [3], in his attempt to accurately approximate the thermal radiation of a blackbody. A blackbody is a perfect absorber of incident electromagnetic radiation. The thermal radiation law has the shape of a left leaning bell curve and accurately describes the energy at all wavelengths. For a blackbody the spectral energy density per frequency increment ($J.m^{-3}.Hz^{-1}$) is given by [4]

$$u(v)dv = \frac{8\pi h}{c^3}\frac{v^3}{e^{hv/k_BT}-1}dv, \tag{1.1}$$

where v, h, and k_B are the frequency, the Planck constant, and the Boltzmann constant respectively. The same notations are used uniformly in the Thesis.

1.2 Radiance PDFs (power and photons) per frequency increment

The radiation power density per frequency increment, $L_v^W(v)$ is found by multiplying by factor of Eq. (1.1) $\frac{c}{4\pi}$. The units are ($J.m^{-2}.Hz^{-1}$).While the photon number density per frequency increment, $L_v^{ph}(v)$ is derived from further division by the photon energy, $E_{ph} = hv$. The units are (number of photons.$m^{-2}.Hz^{-1}$). Both PDFs are found below.

$$L_v^W(v) = \frac{2h}{c^2}\frac{v^3}{e^{hv/k_BT}-1} \tag{1.2a}$$

$$L_v^{ph}(v) = \frac{2}{c^2}\frac{v^2}{e^{hv/k_BT}-1} \tag{1.2b}$$

Using the relation, $v = \frac{c}{\lambda}$, Eq. (1.2) can be expressed in terms of the wavelength, λ:

$$L_v^W(\lambda) = \frac{2hc}{\lambda^3}\frac{1}{e^{hc/k_BT\lambda}-1}, \tag{1.3a}$$

$$L_v^{ph}(\lambda) = \frac{2}{\lambda^2}\frac{1}{e^{hc/k_BT\lambda}-1}. \tag{1.3b}$$

Furthermore, Eqs. (1.3) can be expressed in terms of the wavenumber by using $k = \frac{2\pi}{\lambda}$

$$L_v^W(k) = \frac{\hbar c}{2\pi^2}\frac{k^3}{e^{\hbar kc/k_BT}-1}, \tag{1.4a}$$

$$L_v^{ph}(k) = \frac{1}{2\pi^2}\frac{k^2}{e^{\hbar kc/k_BT}-1}. \tag{1.4b}$$

Where $\hbar$ is the reduced Planck constant. The choice of $\hbar$ is used to establish a common denominator in the coefficient of $2\pi^2$ for both PDFs. This results in the last of the radiance PDFs per frequency increment for a total of six. In summary, there are six PDFs per frequency increment, Eqs. (1.2) - (1.4) considered in this Thesis.

1.3 Radiance PDFs per wavelength increment

Formulation of the spectral energy density for the wavelength is done by substitution of all instances of the spectral variable in Eq. (1.1), including multiplication by the differential $dv = \frac{c}{\lambda^2}d\lambda$. The spectral volume energy density becomes [5],

$$u(\lambda)d\lambda = \frac{8\pi hc}{\lambda^5}\frac{1}{e^{hc/\lambda k_BT}-1}d\lambda. \tag{1.5}$$

With units of (J.m^{-3}.μm^{-1}). Multiplication by $\frac{c}{4\pi}$ once again yields the radiation power density per wavelength, $L_\lambda^W(\lambda)$ with units of (J.s^{-1}.m^{-2}.μm^{-1}). Further division by the energy of the photon returns the photon number density per frequency wavelength, $L_\lambda^{ph}(\lambda)$ in units of (photons. s^{-1}.m^{-2}.μm^{-1}). The frequency must also be replaced in the energy of the photon resulting in division by $\varepsilon_{ph} = \frac{hc}{\lambda}$ rather than the typical $\varepsilon_{ph} = hv$ term. The radiance PDFs per wavelength increment are shown below.

$$L_{\lambda}^{W}(\lambda) = \frac{2\mathrm{hc}^2}{\lambda^5}\frac{1}{e^{hc/\lambda k_B T} - 1} \tag{1.6a}$$

$$L_{\lambda}^{ph}(\lambda) = \frac{2c}{\lambda^4}\frac{1}{e^{hc/\lambda k_B T} - 1} \tag{1.6b}$$

Comparison of Eq. (1.6) and Eq. (1.2) reveals the relationship between the wavelength increment and frequency increment radiance PDFs is nonlinear. This nonlinearity arises from the nonlinear relationship between frequency in wavelength, which translates into analytically distinct PDFs of different powers. The forms of these PDFs are studied further in the following chapter, for now the focus lies on the expression of these PDFs in the other spectral variables. Expression in terms of the frequency returns the following two PDFs,

$$L_{\lambda}^{W}(v) = \frac{2\mathrm{h}}{c^3}\frac{v^5}{e^{hv/k_B T} - 1} \tag{1.7a}$$

$$L_{\lambda}^{ph}(v) = \frac{2}{c^3}\frac{v^4}{e^{hv/k_B T} - 1}. \tag{1.7b}$$

Expression in terms of the wavenumber can be found through substitution of $k = \frac{2\pi}{\lambda}$ into Eq. (1.6) gives,

$$L_{\lambda}^{W}(k) = \frac{\hbar c^2}{8\pi^4}\frac{k^5}{e^{\hbar ck/k_B T} - 1} \tag{1.8a}$$

$$L_{\lambda}^{ph}(k) = \frac{c}{8\pi^4}\frac{k^4}{e^{\hbar ck/k_B T} - 1}. \tag{1.8b}$$

Once again $\hbar$ is used to express the coefficient in terms of $8\pi^4$.

1.4 Radiance PDFs per wavenumber increment

The last spectral variable of interest is the wavenumber. The wavenumber expression is useful as it allows extensions to other areas such as phonon heat capacity which will be discussed in Chapter 4. Expressing the spectral energy density in the wavenumber requires the substitution of the wavenumber $\frac{kc}{2\pi} = v$ and of the differential $dk\frac{c}{2\pi} = dv$ into Eq. (1.1). The spectral energy density expressed in terms of the wavenumber is then given by,

$$u(k)dk = \frac{\hbar c}{\pi^2}\frac{k^3}{e^{\hbar ck/k_B T} - 1}dk. \tag{1.9}$$

This has units of (J.m^{-2}.μm) Using the methods from the previous section the radiation power density, $L_k^W(k)$ in units (J.s^{-1}.m^{-1}.μm) and photon number density, $L_k^{ph}(k)$ in units (photons.s^{-1}.m^{-1}.μm) are expressed per wavenumber increment as shown below,

$$L_k^W(k) = \frac{\hbar c^2}{4\pi^3} \frac{k^3}{e^{\hbar ck/k_B T} - 1} \tag{1.10a}$$

$$L_k^{ph}(k) = \frac{c}{4\pi^3} \frac{k^2}{e^{\hbar ck/k_B T} - 1}. \tag{1.10b}$$

As before Eq. (1.10) through can then be formulated in terms of wavelength and frequency. This results in four more PDFs for a total of 18 PDFs across the three spectral variables. Substitution of $k = \frac{2\pi v}{c}$ results in Eqs. (1.11).

$$L_k^W(v) = \frac{h}{c\pi} \frac{v^3}{e^{hv/k_B T} - 1} \tag{1.11a}$$

$$L_k^{ph}(v) = \frac{1}{c\pi} \frac{v^2}{e^{hv/k_B T} - 1} \tag{1.11b}$$

Further substitution of $v = \frac{c}{\lambda}$ results in the wavelength expression below.

$$L_k^W(\lambda) = \frac{c^2 h}{\pi\lambda^3} \frac{1}{e^{hc/\lambda k_B T} - 1} \tag{1.12a}$$

$$L_k^{ph}(\lambda) = \frac{c}{\pi\lambda^2} \frac{1}{e^{hc/\lambda k_B T} - 1} \tag{1.12b}$$

Finally, now that the spectral energy density has been expressed in terms of frequency, wavelength, and wavenumber as well as their respective increment, and 18 distinct PDFs have been found, we are ready to begin analyzing their form, inflection points, and maxima.

Chapter 2

Analytical Generalization

Comparison of the 18 PDFs through use of dimensionless variables will be covered. The dimensionless variables are used to express the PDFs into groups of similar equations with different coefficients. This allows for a generalization of both PDFs and the solutions to their first and second derivatives. Finally, it allows for the derivation of 52 displacement laws for the various forms of Planck's thermal radiation law.

2.1 Derivation of dimensionless functions

The first unitless variable introduced is for the frequency, and using the introduced notations (vide supra) is defined as

$$x = \frac{hv}{k_B T}. \tag{2.1}$$

Using Eq. (2.1) the six PDFs as a function of v can be rewritten in terms of the unitless variable x, see Table 1. Where n is the power of x, and C is the coefficient independent of $k_B T$ and x

Table 1. Summary of the six PDFs as a function of photon frequency, v, in the unitless variable $x = hv/k_B T$, the power, the coefficient, and the equation number, are listed as well.

Notation	Unitless Form	n	C	
$L_v^{ph}(x,T)$	$C_v\left(\frac{x^2}{e^x-1}\right)(k_B T)^2$	2	$\frac{2}{(hc)^2}$	(1)
$L_v^{w}(x,T)$	$C_v\left(\frac{x^3}{e^x-1}\right)(k_B T)^3$	3		(2)
$L_\lambda^{ph}(x,T)$	$C_\lambda\left(\frac{x^4}{e^x-1}\right)(k_B T)^4$	4	$\frac{2c}{(hc)^4}$	(3)
$L_\lambda^{w}(x,T)$	$C_\lambda\left(\frac{x^5}{e^x-1}\right)(k_B T)^5$	5		(4)
$L_k^{ph}(x,T)$	$C_k\left(\frac{x^2}{e^x-1}\right)(k_B T)^2$	2	$\frac{c}{(hc)^2\pi}$	(5)
$L_k^{w}(x,T)$	$C_k\left(\frac{x^3}{e^x-1}\right)(k_B T)^3$	3		(6)

The second unitless variable introduced is for the wavelength, and is defined as:

$$\tilde{x} = \frac{\lambda k_B T}{hc}. \tag{2.2}$$

Using Eq. (2.2) the six PDFs as a function of λ can be rewritten in terms of the unitless variable $\tilde{x}$. Leading to six more unitless PDFs found in Table 2.

Table 2. Summary of the six PDFs as a function of photon frequency, λ, in the unitless variable $\tilde{x} = \lambda k_B T/hc$, the power, the coefficient, and the equation number, are listed as well.

Notation	Unitless Form	n	C	PDF
$L_v^{ph}(\tilde{x},T)$	$C_v\left(\frac{\tilde{x}^{-2}}{e^{1/\tilde{x}}-1}\right)(k_B T)^2$	2	$\frac{2}{(hc)^2}$	(7)
$L_v^{w}(\tilde{x},T)$	$C_v\left(\frac{\tilde{x}^{-3}}{e^{1/\tilde{x}}-1}\right)(k_B T)^3$	3		(8)
$L_\lambda^{ph}(\tilde{x},T)$	$C_\lambda\left(\frac{\tilde{x}^{-4}}{e^{1/\tilde{x}}-1}\right)(k_B T)^4$	4	$\frac{2c}{(hc)^4}$	(9)
$L_\lambda^{w}(\tilde{x},T)$	$C_\lambda\left(\frac{\tilde{x}^{-5}}{e^{1/\tilde{x}}-1}\right)(k_B T)^5$	5		(10)
$L_k^{ph}(\tilde{x},T)$	$C_k\left(\frac{\tilde{x}^{-2}}{e^{1/\tilde{x}}-1}\right)(k_B T)^2$	2	$\frac{c}{(hc)^2\pi}$	(11)
$L_k^{w}(\tilde{x},T)$	$C_k\left(\frac{\tilde{x}^{-3}}{e^{1/\tilde{x}}-1}\right)(k_B T)^3$	3		(12)

The wavenumber-unitless variable introduced is defined as

$$\bar{x} = \frac{\hbar c k}{k_B T}. \tag{2.3}$$

Using Eq. (2.3) the six PDFs as a function of v can be rewritten in terms of the unitless variable $\bar{x}$, see Table 3.

Table 3. Summary of the six PDFs as a function of photon frequency, k, in the unitless variable $\bar{x} = \hbar ck/k_B T$, the power, the coefficient, and the equation number, are listed as well.

Notation	Unitless Form	n	C	PDF
$L_v^{ph}(\bar{x},T)$	$C_v\left(\frac{\bar{x}^2}{e^{\bar{x}}-1}\right)(k_BT)^2$	2	$\frac{2}{(hc)^2}$	(13)
$L_v^{w}(\bar{x},T)$	$C_v\left(\frac{\bar{x}^3}{e^{\bar{x}}-1}\right)(k_BT)^3$	3		(14)
$L_\lambda^{ph}(\bar{x},T)$	$C_\lambda\left(\frac{\bar{x}^4}{e^{\bar{x}}-1}\right)(k_BT)^4$	4	$\frac{2c}{(hc)^4}$	(15)
$L_\lambda^{w}(\bar{x},T)$	$C_\lambda\left(\frac{\bar{x}^5}{e^{\bar{x}}-1}\right)(k_BT)^5$	5		(16)
$L_k^{ph}(\bar{x},T)$	$C_k\left(\frac{\bar{x}^2}{e^{\bar{x}}-1}\right)(k_BT)^2$	2	$\frac{c}{(hc)^2\pi}$	(17)
$L_k^{w}(\bar{x},T)$	$C_k\left(\frac{\bar{x}^3}{e^{\bar{x}}-1}\right)(k_BT)^3$	3		(18)

In summary, three different unitless variables are adopted (i) $x = hv/k_BT$, (ii) $\tilde{x} = \lambda k_BT/hc$, (iii) $\bar{x} = \hbar ck/k_BT$, with the purpose of evaluating the positions of the three characteristic points, discussed in detail in 2.2.

The 18 equations presented above are grouped based on the function dependence , x, $\tilde{x}$, $\bar{x}$. Furthermore, the same equations can be grouped by:

(i) the increment of the PDFs:

- v-PDFs ($L_v^W(x)$, $L_v^{ph}(x)$, $L_v^W(\bar{x})$, $L_v^{ph}(\bar{x})$, $L_v^W(\tilde{x})$, $L_v^{ph}(\tilde{x})$)
- λ- PDFs ($L_\lambda^W(x)$, $L_\lambda^{ph}(x)$, $L_\lambda^W(\bar{x})$, $L_\lambda^{ph}(\bar{x})$, $L_\lambda^W(\tilde{x})$, $L_\lambda^{ph}(\tilde{x})$)
- k- PDFs ($L_k^W(x)$, $L_k^{ph}(x)$, $L_k^W(\bar{x})$, $L_k^{ph}(\bar{x})$, $L_k^W(\tilde{x})$, $L_k^{ph}(\tilde{x})$)

(ii) the power index, n:

- n = 2 ($L_v^{ph}(x)$, $L_k^{ph}(x)$, $L_v^{ph}(\bar{x})$, $L_k^{ph}(\bar{x})$, $L_v^{ph}(\tilde{x})$, $L_k^{ph}(\tilde{x})$)

- n = 3 ($L_v^W(x)$, $L_k^W(x)$, $L_v^W(\bar{x})$, $L_k^W(\bar{x})$, $L_v^W(\tilde{x})$, $L_k^W(\tilde{x})$)
- n = 4 ($L_\lambda^{ph}(x)$, $L_\lambda^{ph}(\bar{x})$, $L_\lambda^{ph}(\tilde{x})$)
- n = 5 ($L_\lambda^W(x)$, $L_\lambda^W(\bar{x})$, $L_\lambda^W(\tilde{x})$)

The coefficients are evaluated up to two decimal places, in the convenient, at atomic scale, units of energy and length - eV, μm:

(i) for v-PDFs are $C_v = 1.30\ eV^{-2}\mu m^{-2}$,

(ii) for λ-PDFs $C_\lambda = 2.54 \times 10^8\ eV^{-4}s^{-1}\mu m^{-3}$, and

(iii) for the k-PDFs $C_k = 6.20 \times 10^{13} eV^{-2}s^{-1}\mu m^{-1}$.

The discussion continues with grouping the functions by variables:

(i) $x = hv/k_BT$, PDF (v), see Table 1

(ii) $\tilde{x} = \lambda k_BT/hc$, PDF ($\lambda$), see Table 2

(iii) $\bar{x} = \hbar ck/k_BT$, PDF(k), see Table 3

Comparing PDF (v) and PDF (λ), the numerical values for n (2, 3, 4, 5) differ by sign. This is attributed to the nonlinear relationship between frequency and wavelength ($v = c/\lambda$) , see Tables 1, 2. PDF(k) and PDF(v) unitless presentations have all positive powers of the variables due to the linear relationship between the frequency and wavenumber ($v = ck/2\pi$), see Tables 1, 3. Another consequence of the linear relationship between k, v, are that the first two and last two PDFs in each table differ in constant only. Thus, analysis of the v-PDFs is the same as analysis of the k-PDFs.

Thus, the total number of analytically unique PDFs is reduced to eight equations in two groups: (i) four v-PDFs; and (ii) four λ-PDFs. These eight PDFs will be the focus of the thesis moving forward. Based on the discussion above, a general form of the eight total v-PDFs and λ-PDFs representations of Planck's thermal radiation law can be proposed:

$$ {}^nL(u,T) = C\left(\frac{u^n}{e^u - 1}\right)(k_BT)^n, \tag{2.4}$$

where for $n = 2,3,4,5$, $u = \begin{cases} x = hv/k_B T \\ 1/\tilde{x} = hc/\lambda k_B T \end{cases}$,

while $C = \begin{cases} C_v = 1.30\, eV^{-2}\mu m^{-2}, & if\ n = 2,3 \\ C_\lambda = 2.54 \times 10^8\ eV^{-4}s^{-1}\mu m^{-3}, & if\ n = 4,5 \end{cases}$.

Eq. (2.4) can be extended to the other 10 PDFs by replacing x with $\bar{x}$, and the coefficients with C_k for the wavenumber PDFs.

2.2 Characteristic points: derivation and solving the transcendental equations

The purpose of this section is to derive a set of transcendental equations for the v-PDFs and λ-PDFs representations of Planck's thermal radiation law and find the solutions. The transcendental equations come from taking the first and second derivative of the v-PDFs and λ-PDFs, then solving for the roots. The total number of transcendental equations is 16; eight for the first derivative, and eight for the second derivative. This section will present the general form and the roots (total of 23-characteristic points) for each type of transcendental equation. As will be explored in Chapter 3, the roots are in fact constants of displacement laws.

The first set of transcendental equations is found by differentiation of Eq. (2.4) for the variable x. The second set are found through differentiation of Eq. (2.4) for the variable $\tilde{x}$. The roots were solved using Newton's method for numerically approximating roots. The transcendental equations and roots are summarized in Table 4 for ${}^n L(x)$ and in Table 5 for ${}^n L(\tilde{x})$. The result is a total of eight characteristic points corresponding to peak positions. The solutions presented are only to the three decimal places. It is important to note that an exact solution (within $< 10^{-6}$) to the transcendental equations usually require 5 to 14 decimal places, See Appendix A for full precision, and derivation of roots.

Table 4. Summary of the transcendental equations, derived from ${}^n L(x)$, $x = hv/kT$, and their solutions x_{-i}; x_o; x_{+i}.

${}^n L(x)$	Transcendental equations	$IP_L,\ x_{-i}$	$Peak,\ x_o$	$IP_R,\ x_{+i}$
${}^2 L(x)$	$(x-2)e^x + 2 = 0$		1.594	
	$\left(x^2 - 4x + 2\right)e^{2x} + \left(x^2 + 4x - 4\right)e^x + 2 = 0$	0		3.086

${}^{3}L(x)$	$(x-3)e^{x}+3=0$		2.821	
	$(x^{2}-6x+6)e^{2x}+(x^{2}+6x-12)e^{x}+6=0$	0.966		4.623
${}^{4}L(x)$	$(x-4)e^{x}+4=0$		3.921	
	$(x^{2}-8x+12)e^{2x}+(x^{2}+8x-24)e^{x}+12=0$	1.855		5.961
${}^{5}L(x)$	$(x-5)e^{x}+5=0$		4.965	
	$(x^{2}-10x+20)e^{2x}+(x^{2}+10x-40)e^{x}+20=0$	2.699		7.222

Table 5. Summary of the transcendental equations, derived from ${}^{n}L(\tilde{x})$, $\tilde{x}=\lambda kT/hc$, and their solutions $\tilde{x}_{-i};\ \tilde{x}_{o};\ \tilde{x}_{+i}$.

${}^{n}L(\tilde{x})$	Transcendental equations	$IP_L,\ \tilde{x}_{-i}$	$Peak,\ \tilde{x}_{o}$	$IP_R,\ \tilde{x}_{+i}$
${}^{2}L(\tilde{x})$	$(1-2\tilde{x})e^{1/\tilde{x}}+2\tilde{x}=0$		0.628	
	$(6\tilde{x}^{2}-6\tilde{x}+1)e^{2/\tilde{x}}+(-12\tilde{x}^{2}+6\tilde{x}+1)e^{1/\tilde{x}}+6\tilde{x}^{2}=0$	0.216		1.035
${}^{3}L(\tilde{x})$	$(1-3\tilde{x})e^{1/\tilde{x}}+3\tilde{x}=0$		0.354	
	$(12\tilde{x}^{2}-8\tilde{x}+1)e^{2/\tilde{x}}+(-24\tilde{x}^{2}+8\tilde{x}+1)e^{1/\tilde{x}}+12\tilde{x}^{2}=0$	0.168		0.539
${}^{4}L(\tilde{x})$	$(1-4\tilde{x})e^{1/\tilde{x}}+4\tilde{x}=0$		0.255	
	$(20\tilde{x}^{2}-10\tilde{x}+1)e^{2/\tilde{x}}+(-40\tilde{x}^{2}+10\tilde{x}+1)e^{1/\tilde{x}}+20\tilde{x}^{2}=0$	0.138		0.371
${}^{5}L(\tilde{x})$	$(1-5\tilde{x})e^{1/\tilde{x}}+5\tilde{x}=0$		0.201	
	$(30\tilde{x}^{2}-12\tilde{x}+1)e^{2/\tilde{x}}+(-60\tilde{x}^{2}+12\tilde{x}+1)e^{1/\tilde{x}}+30\tilde{x}^{2}=0$	0.118		0.284

The general form of the transcendental equations associated with ${}^{n}L(x)$, where $x=hv/k_BT$, for n = 2, 3, 4, 5 is suggested as:

$$(x-n)e^{x}+n=0 \tag{2.5a}$$

$$(x^{2}-2nx+n(n-1)e^{2x}+(x^{2}+2nx-2n(n-1))e^{x}+n(n-1)=0. \tag{2.5b}$$

The general form of the transcendental equations associated with ${}^{n}L(\tilde{x})$, where $\tilde{x}=\lambda kT/hc$, for n = 2, 3, 4, 5 is suggested as:

$$(1-n\tilde{x})e^{1/\tilde{x}}+n\tilde{x}=0 \tag{2.6a}$$

$$(n(n+1)\tilde{x}^{2}-2(n+1)\tilde{x}+1)e^{2/\tilde{x}}+(-2n(n+1)\tilde{x}^{2}+2(n+1)\tilde{x}+1)e^{1/\tilde{x}}+n(n+1)\tilde{x}^{2}=0. \tag{2.6b}$$

Chapter 3

Comparative Analysis and Discussion of the Inflection Points and Maxima

The focus of this chapter will be analysis of the transcendental equations and their roots, where each root can be interpreted as a constant for a displacement law (Section 3.1). The symmetric properties of Planck's thermal radiation law will be addressed through (i) a proposed IP standard deviation, (ii) radiance and temperature dependence at the characteristic points, (iii) the ratio of the slopes, and (iv) integral area between the inflection (special) points.

3.1 Displacement laws and temperature sensitivity of the characteristic points

The goal of this section is to derive displacement laws by using the solutions to the transcendental equations in Chapter 2.2. The term "displacement law" comes from Wien's displacement law, the inspiration for this thesis. Wien's displacement law states that the peak spectral radiance of the blackbody radiation per unit wavelength is given by [6], $\lambda_{peak} = \frac{b}{T}$, where λ_{peak} is the wavelength at the peak radiance, and b is Wien's displacement constant ($b = 2.89 \times 10^3 [\mu m. K]$). This thesis proposes that the characteristic points of the PDFs serve as constants functioning identically to Wien's displacement constant. The proposed new constants (total of 52) based on the roots of the transcendental equations, $x_{o(\pm i)}$ $\tilde{x}_{o(\pm i)}$, (total of 23) summarized in Tables 4 and 5.

Using Eq. (2.1) - (2.3), the suggested temperature displacement constants are in terms of; (i) photon energy ($\varepsilon = hv$) $\varepsilon[eV] = x_{o(\pm i)}(k_B T) = 8.62 \times 10^{-5} [eV. K^{-1}] x_{o(\pm i)} T$; (ii) wavelength $\lambda[\mu m] = \tilde{x}_{o(\pm i)} \frac{hc}{k_B T} = 1.44 \times 10^4 [\mu m. K] \frac{\tilde{x}_{o(\pm i)}}{T}$; and (iii) wavenumber $k[\mu m^{-1}] = \frac{x_{o(\pm i)} k_B T}{\hbar c} = 4.36 \times 10^{-4} [K^{-1}. \mu m^{-1}] \frac{x_{o(\pm i)}}{T}$. For example, using $\tilde{x}_o = 0.201$, see Table 4, yields $\lambda T = 2.89 \times 10^3 [\mu m. K]$ which is the well-known Wien's displacement constant.

A total of 18 PDFs have been derived from the unitless variables,(see Tables 1 – 3), and 52 displacement laws proposed for the different mathematical forms of Planck's Law.

3.2 Statistical standard deviation (width of the distribution) and its temperature sensitivity

The Gaussian (normal) distribution is a well-known probability density function, characterized by the symmetry about its peak. The symmetry arises from the equidistant inflection points to the peak. The Gaussian distribution is given by,

$$f(x) = \frac{1}{\sigma\sqrt{2\pi}} e^{-\frac{1}{2}\left(\frac{x-\mu}{\sigma}\right)^2} \tag{3.1}$$

where σ is the standard deviation, and μ is the mean [7]. The rule states that 68% of the observed values fall within one standard deviation, 95% within two standard deviations, and 99.7% within three standard deviations [7] The inflection points of the normal distribution are located at the first standard deviation [8]. Planck's thermal radiation law shares a similar bell curve shape and is pseudo symmetric. The symmetry of the Gaussian distribution serves as the basis for proposing a similar standard deviation based on the inflection points of the thermal radiation law. This section aims to define this standard deviation, discuss its sensitivity to temperature, and compare it with the usual statistical standard deviation.

The right and left inflection points are used in defining the standard deviation for the thermal radiation distribution (herein referred to as the IP standard deviation). The position relative to the peak of the IP standard deviation is defined as: (i) $x_o - x_{-i}$ and $x_{+i} - x_o$ for ${}^nL(x)$; (ii) $\tilde{x}_o - \tilde{x}_{-i}$ and $\tilde{x}_{+i} - \tilde{x}_o$ for ${}^nL(\tilde{x})$. Comparison of the statistical standard deviation, σ is now necessary. The relative positions of were found by locating the position at the radiance one statistical standard deviation on either side of the peak. The relative for the left and right positions of one σ from the peak are defined as: (i) σ_{-i} or $\tilde{\sigma}_{-i}$ for ${}^nL(x)$ and (ii) σ_{+i} or $\tilde{\sigma}_{+i}$ for ${}^nL(\tilde{x})$. The ratio: (i) $(x_o - x_{-i})/(x_{+i} - x_o)$, was found to be between 1.07 – 1.01 compared to 0.648 - 0.777 for σ_-/σ_+, while (ii) $(\tilde{x}_o - \tilde{x}_{-i})/(\tilde{x}_{+i} - \tilde{x}_o)$, was found to be 1.01 compared with 0.411 – 0.795 for $\tilde{\sigma}_-/\tilde{\sigma}_+$. Further comparison can be made by plotting the two parameters against each other and fitting with a line of best fit, see Fig. 1. The slope of these lines quantifies the divergence in numerical values between parameters. A slope approaching unity signifies a small difference in values, whereas a slope differing from unity implies a greater difference in values. The ratio of the relative positions of the IP standard deviations shows support that

defining the inflection points as a IP standard deviation is appropriate due to symmetry. A comparison of the statistical and inflection point parameters is found in Table B.1, B.2.

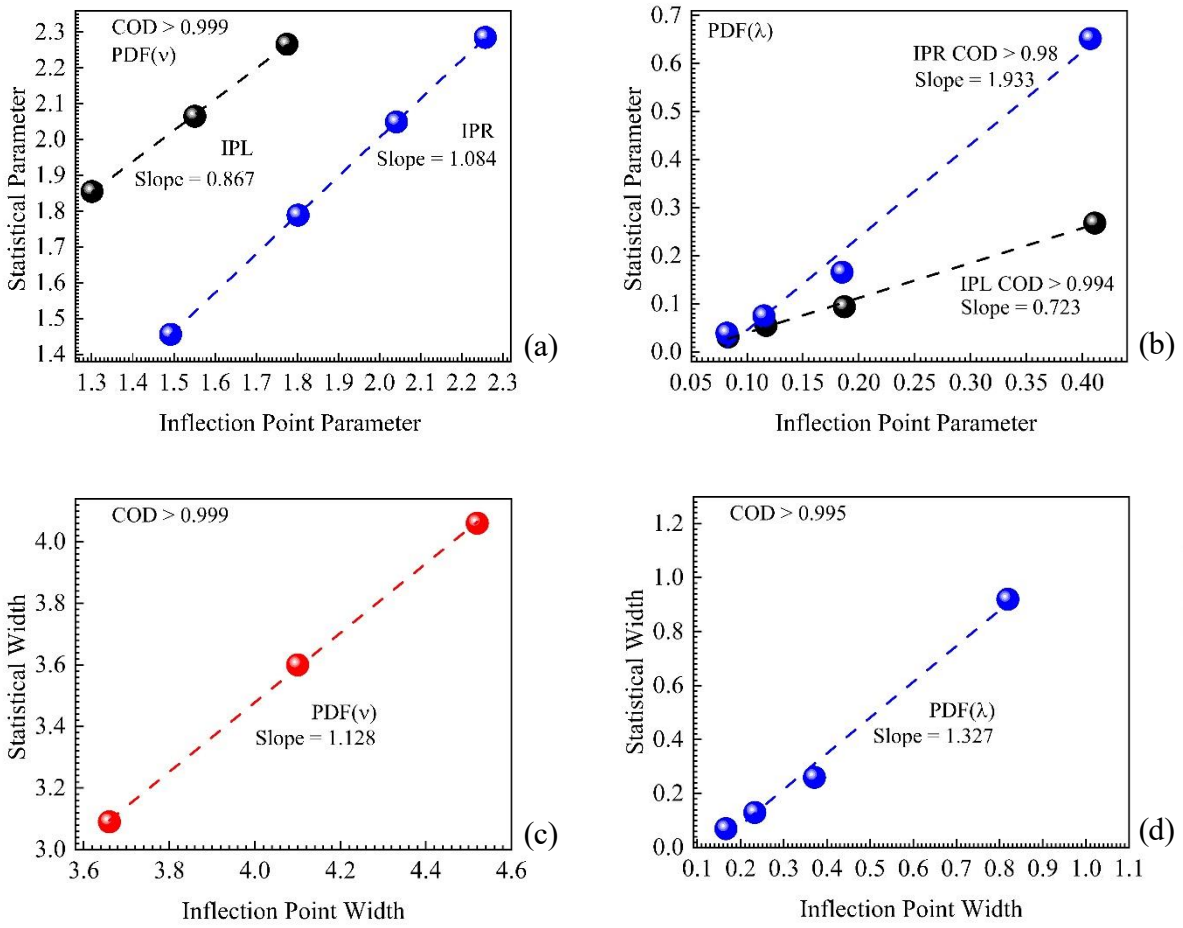

Figure 1. The statistical parameters (y axis) are plotted vs. the inflection point parameters (x axis) and fitted linearly (COD listed within the figure). (a) Comparison of the relative positions from the peak of the standard deviations of PDF(v). Similarly (b) for PDF(λ). The width of the distributions; (c) for PDF(v), and (d) for PDF(λ).

The width of the thermal radiation distribution can be defined as: (i) photon energy span (in eV) between inflection points, $\Delta\varepsilon = (x_{+i} - x_{-i})k_BT$ for ${}^nL(x)$, and (ii) wavelength span (in nm) $\Delta\lambda = (\tilde{x}_{+i} - \tilde{x}_{-i})hc/k_BT$ for ${}^nL(\tilde{x})$. For example, approximating the temperature of the Sun to be T=5800K, then k_BT=0.5 eV. This shows that $\Delta\varepsilon$ can vary up to 47%, depending on the function used. The distribution widths scale linearly with temperature. On the other hand, the wavelength width for the distribution as a function of wavelength can vary up to 5x depending

on the distribution. The distributions per unit wavelength have smaller standard deviations and as such have narrower widths. The widths are inversely proportional to the temperature and decrease non-linearly with the temperature, see Table B.2.

The sensitivity of the inflection points is due to the magnitude of the displacement constant. The right point is the most sensitive of the points, see Tables 4, 5. The set of points corresponding to ${}^{5}L(x)$ and ${}^{2}L(\tilde{x})$ represent the most sensitive points, while points with the least sensitivity correspond to ${}^{2}L(x)$ and ${}^{5}L(\tilde{x})$. Fig. 2(a) reveals a strong linear correlation (Pearson's r > 0.997) with the power index in the case of ${}^{n}L(x)$. Fig. 2(b) shows a strong power law decay of the characteristic points with temperature (Coefficient of Determination, COD > 0.995) with increasing power index for ${}^{n}L(\tilde{x})$.

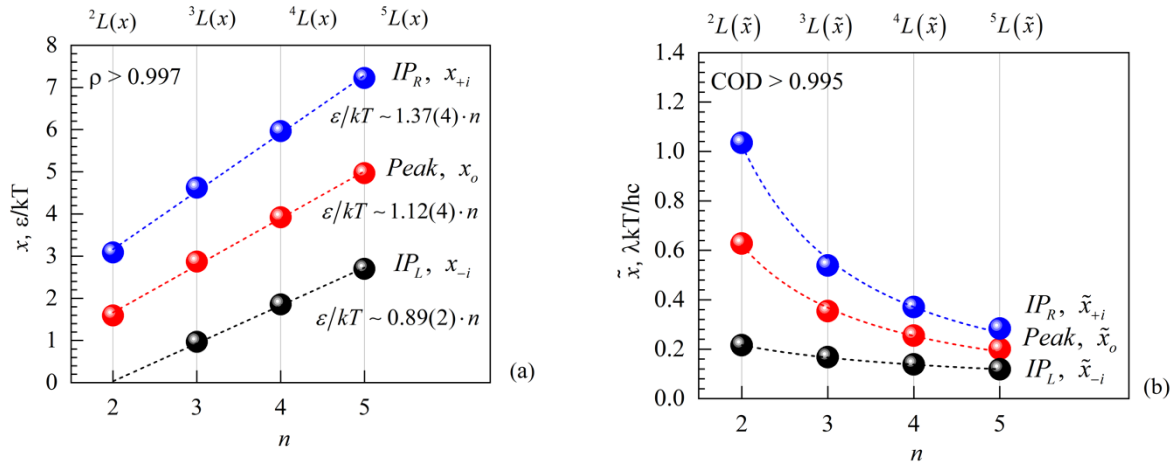

Figure 2. Summary of the positions of the characteristic points (y axis) of the distribution functions (indicated at the top, at the vertical reference lines), correlated to the power index n. The short dash line in (a) is a linear fit, the slopes and the Pearson's r factor are listed. The dashed lines in (b) are guide to the eye.

Overall, the slopes of the fitted lines paired with the numerical differences discussed previously show that defining the inflection points as the IP standard deviation is not typically suitable. However, there is strong support for defining the position of the right inflection point as one standard deviation from the peak. Fig. 1(a) shows that the slope is approximately unity for the fit of IPR and of PDF(v). Furthermore, the values differ 0.4-2.5% between the statistical and inflection point standard deviation parameters. The original assumption that Planck's thermal

radiation law shares symmetrical elements with the Gaussian distribution could be a possible explanation. The Gaussian distribution peak is centered at the mean and falls to zero at infinity in either direction. Planck's thermal radiation law falls to zero at infinity only right of the peak, it falls to zero for zero wavelength or frequency on the left. This could explain why the IPR appears to be located at one σ from the peak.

3.3 Temperature dependence of the radiance at the characteristic points

So far, the thesis has been centered on the position of the three characteristic points for each PDF. This section shifts focus to the radiance at the characteristic points. Like the position, the temperature dependence of the radiance will be discussed. The ratio between the radiance of the characteristic points will also be discussed.

The radiance of the characteristic points is defined by Eq. (2.4), restated below,

$$ {}^{n}L(u,T) = C\left(\frac{u^n}{e^u - 1}\right)(k_B T)^n, \tag{2.4}$$

where for $n = 2,3,4,5$, $u = \begin{cases} x = hv/k_B T \\ 1/\tilde{x} = hc/\lambda k_B T \end{cases}$,

while $C = \begin{cases} C_v = 1.30\ eV^{-2}\mu m^{-2}, & if\ n = 2,3 \\ C_\lambda = 2.54 \times 10^8\ eV^{-4}s^{-1}\mu m^{-3}, & if\ n = 4,5. \end{cases}$

The radiance for all characteristic points can be seen in Table B.3, B.4. It is important to take care in interpreting the radiance for each unitless variable and power index. For example, the peak radiance of ${}^{2}L(x)$ is $0.211\ photons.\mu m^{-2}$, while for ${}^{5}L(x)$ is $1.682 \times 10^8\ eV.s^{-1}.\mu m^{-3}$. This is due to the definition of each PDF discussed in Chapter 1. The radiance of each inflection point is not only different in its definition but in its temperature sensitivity. The radiance of the right inflection point (IPR) is more sensitive to temperature than the radiance of the left inflection point (IPL). The temperature sensitivity of the radiances arises from the temperature sensitivity (discussed in Section 3.2) of the inflection points. The greater the sensitivity of the critical points, the greater the sensitivity of the radiance.

The ratio IPL/IPR of the radiance is also important. The radiance at the IPR point is greater than at the IPL, see Table B.3, B.4. Furthermore, the rate at which the radiance at the IPR

increases is greater than the rate at which the radiance at the IPL increases, see Fig. 3(a). The IPR radiance is stable, always being roughly 70% the value of the peak radiance for the PDF (v)'s. The IPL radiance is also stable across the various forms of Planck's thermal radiation law, being roughly 40-50% of the peak radiance for both PDF (v)'s and PDF (λ)'s. The ratio common ratios between IPR, IPL radiance and the peak radiance in the PDF (v)'s, support symmetrical considerations discussed in Section 3.1. Conversely, the spread in ratios for the PDF (λ) further reinforce the non-symmetric structure of this form of Planck's thermal radiation law.

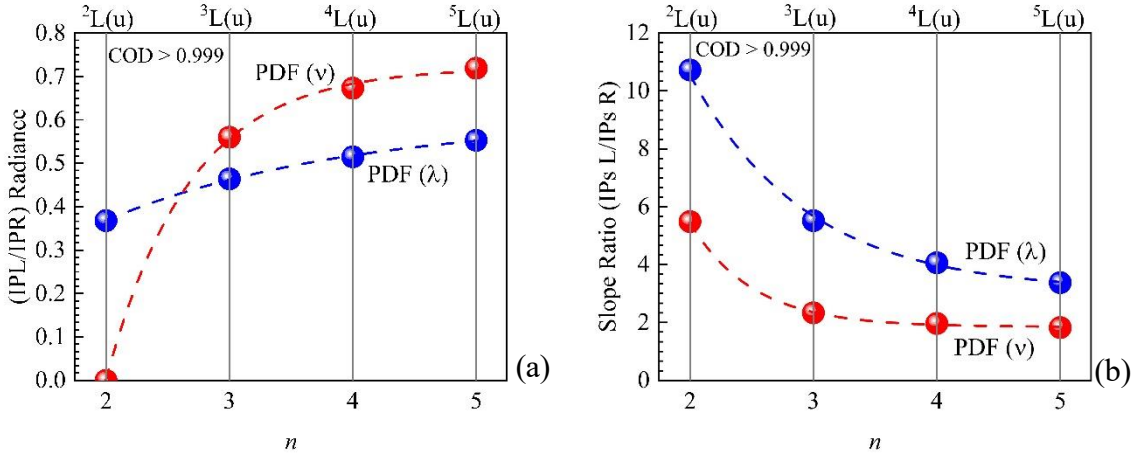

Figure 3. The graphs denote the PDF (v) in red, and the PDF (λ) in blue. All points were fitted with an exponential decay function CODs shown. (a) Summary of the ratio IPL/IPR Radiance (y axis) for the distribution functions (indicated at the top, at the vertical reference lines) correlated by the power index n. (b) Summary of the slope ratio IPsL/IPsR (y axis) for the distribution functions correlated by power index n. The dashed lines are a guide to the eye.

3.4 Ratio of the slopes at the inflection points

Having discussed the position of the inflection points and their radiance, it is important to also discuss the slopes of the characteristic points. The peak position will have a slope of zero, so focus shifts to the inflection points. The slopes alone give little information, so the ratio of the slopes is also analyzed. Fig. 3(b) shows the slopes of the left and right inflection points plotted against the power index, n. It can be seen from the figure that the slope of the left inflection point is always greater in magnitude than the slope of the right inflection point. As a result, the ratio between the left and right slopes is greater than one for all n. The ratio remains rather constant for ${}^nL(x)$ having values between 1.8-2.3 however, for ${}^nL(\tilde{x})$ the ratio decreases greatly from

10.7-3.4 with increasing powers of n. The set of ${}^{n}L(x)$ probability distributions preserve the symmetry as indicated but the slope ratios. For numerical values of the slopes and the ratio see Table B.5., B.6.

3.5 Integral between the IPs of the area-normalized functions

This section focuses on the final comparison parameters, the central integral radiance (CIR) based on the inflection points, and the statistical central integral radiance (SCIR) for ${}^{n}L(x)$ and ${}^{n}L(\tilde{x})$, considered separately.

First, we consider ${}^{n}L(x)$. The central integral radiance is defined as the ratio of the area bound between x=0 - 25 and the area bound by the inflection points. Both CIR (blue bullet points) and SCIR (black bullet points) are plotted vs. the power index in Fig. 4a. For functions of the form, ${}^{n}L(x)$ the central integral radiance is ~ 66 % of the whole, while the SCIR is ~ 60%, a little less than two thirds, Table B.7. These numbers agree with the established fact that the left sigma ($\sigma\_$) is closer to the peak compared to the IPL, ($x_o - x_{\_i}$), see Table B.1 (columns 2 and 6) This similarity is seen in Fig. 4(a), where the CIR and SCIR were approximately fit linearly with slopes ≤ 0.01. The percent difference between the CIR and SCIR values is ~10 % while in the Gaussian distribution, Eq, (3.1) if CIR and SCIR values are calculated, they will be identical and equal to ~68 %. The Gaussian distribution value is about ~3 % higher than the CIR value (~ 66 %) and ~12 % higher than the SCIR value of the Planck's thermal radiation functions. This serves as support for the definition of the IP standard deviation proposed in 3.2.

Next, we consider ${}^{n}L(\tilde{x})$. It is of note that the CIR values assessed for functions ${}^{n}L(\tilde{x})$ appear to increase with the power index, n. CIR values increase from 14.6% to 46.8% , revealing ~30 % increase, illustrated in Fig. 4b, red bullet points. SCIR values assessed for functions ${}^{n}L(\tilde{x})$ are less than the CIR values and appear to slightly increase from 16.9% to 22.3% (~6 %) with the power index, n. ${}^{n}L(\tilde{x})$ being obtained via non-linear variable transformation has less symmetry elements, see section 3.1.

Overall, it appears that ${}^{n}L(x)$ –set of functions share more symmetry elements with the Gaussian distribution compared to the ${}^{n}L(\tilde{x})$-set of functions.

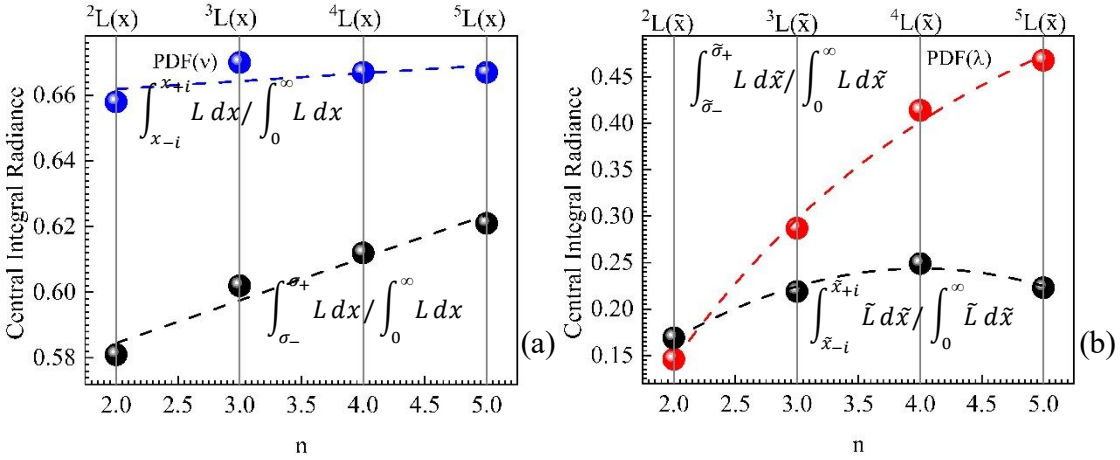

Figure 4. Summary of the CIR and SCIR (y axis) plotted vs. the power index n (x axis). (a) for ${}^nL(x)$, and (b) for ${}^nL(\tilde{x})$. The dashed lines are a guide to the eye.

Chapter 4

Applications and Future Work

In the previous chapters discussion has focused on the generalization, characteristic points, and properties of the various forms of Plack's thermal radiation law. This chapter will instead focus on the applications of these functions in Photobiology, and future work in phonon heat capacity.

4.1 Applications in Photobiology

Planck's thermal radiation law has been presented in 18 forms for three spectral variables, eight of which have distinct analytical forms. If all forms are descriptions of the same thing, which form should be used? This section aims to address a case where some forms may be more suitable for use than others.

The radiance PDFs can be expressed in terms of frequency, wavelength, and wavenumber, the radiance PDFs can further be presented for either photon number density or radiant power density. In nature bio-photochemical reactions use the energy delivered by the photon. Both the wavelength and wavenumber are artificial units created by scientists to quantify properties of photons, however the energy of the photon, while quantified in eV or J, is a more natural quantity. Thus, only the PDF(v) (frequency can be linearly transformed into photon energy) will be discussed moving forward.

Fig. 5(a) compares the area normalized Planck distributions per frequency increment to the usable energy range of bio-photochemical reactions shaded in gray. The photon energy ranges shown are those of chlorophyl a [9] (green solid line) and phycoerythrin [10] (purple solid line). The three characteristic points, inflection point and peak positions, are used as comparison criteria for the four forms shown in Fig. 5(a). These characteristic points are chosen as comparison criteria due to their well-defined positions in each representation. Fig. 5(b) illustrated the percentage of biophoton energies that fall within the IP range. The IP separation varies from 1.5 eV (n=2) to 2.3 eV (n=5). Furthermore, the peak shifts to higher photon energies as the power index increases. The locations of the peak for: (i) n=2 is 0.8 eV, (ii) n=3 is 1.4 eV, (iii) n=4 is 1.9 eV, and (iv) n=5 is 2.5 eV. As seen in Fig. 5(b), the peak for the n=2 PDF is not within

the biophoton range of 1.2-3 eV. The peak of n=3 is within the biophoton range but close to the lower bound. The peaks of n=4,5 are well within the bounds.

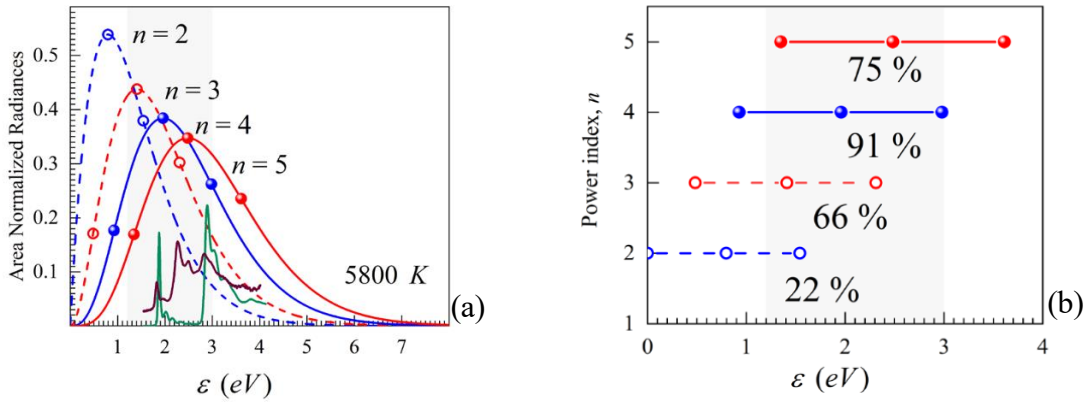

Figure 5. (a) The area-normalized Planck's spectra as a function of energy, ε, at 5800 K, labeled by the power index n. The absorption spectra of chlorophyl a [9] (green solid line) and phycoerythrin [10] (purple solid line) is shown below the PDFs. (b) The peak and inflection points positions are plotted at the corresponding power index (y axis), with the percent of biophotons that fall within the IP range listed in the figure. The shaded area in both graphs illustrates the biophoton range discussed.

Further comparison is done by analyzing the percentage of biophotons that fall within the IP range of the PDF(v)'s. Illustrated in Fig. 5(b), the percent of biophotons within the IP range of the n=2 and n=3 is 22% and 66% respectively, while it is 91% for n=4 and 75% for n=5. The n=2 PDF has poor association with the biophoton energies, having only 22% of the biophoton range fall within its inflection points. The n=3,5 PDF's have similar percentages of 66% and 75% respectively. The photon radiance PDF per wavelength increment (n=4) has the highest percentage of biophotons falling within its inflection point range at 91%. This shows that while all four PDFs are correct representations of Planck's thermal radiation law, Fig. 5(b) suggests that the biophoton's energy range of 1.2-3 eV is synergistic with Planck's thermal radiation law described as photon radiance per wavelength increment (n=4).

4.2 Future work in Solid-State Physics: energy and heat capacity of phonons

This section aims to provide an outline for future work by extending the generalization proposed to the field of Solid-State Physics. The thesis has focused on Planck's thermal radiation law, and by extension photons, proposing generalizations of the various analytical forms and positions of their characteristic points. As Planck's law is derived from the Planck distribution (see Introduction) for a photon gas, it is possible the generalizations could be extended to other functions derived from the Planck distribution.

Phonons are excitations in a periodic lattice of atoms or molecules. Phonons are a type of quasiparticle that quantizes type of elastic (crystal lattice) standing waves in materials, like the quantized light waves called photons [11]. The Planck distribution (stated below for phonons) can be used in calculating the energy and heat capacity of phonons. The energy of a collection of photons (or lattice energy) in thermal equilibrium can be found by multiplication of Eq. (4.1) with the phonon energy $\hbar\omega$, and

$$n = \frac{1}{e^{\frac{\hbar\omega}{k_B T}} - 1} \tag{4.1}$$

summing over all modes, yielding

$$U = \sum_p \sum_K \frac{\hbar\omega}{e^{\frac{\hbar\omega}{k_B T}} - 1}. \tag{4.2}$$

The summation over K modes can be replaced with an integral of the number of modes per unit frequency range, $D_p(\omega)$ resulting in

$$U = \sum_p \int d\omega D_p(\omega) \frac{\hbar\omega}{e^{\frac{\hbar\omega}{k_B T}} - 1}. \tag{4.3}$$

For a constant sound velocity, the density of states can be written as $D_p(\omega) = V\omega^2/2\pi^2\nu^3$,where V is the volume, and ν is the speed [11]. Combined with Eq. (4.3) the total energy U is given by

$$U = \int_0^{\omega_D} d\omega \left(\frac{V\omega^2}{2\pi^2\nu^3}\right)\left(\frac{\hbar\omega}{e^{\hbar\omega/k_B T} - 1}\right). \tag{4.4}$$

Here ω_D is the cutoff frequency, meaning frequencies greater than this are forbidden. As in Chapter 2 we can propose a unitless variable

$$z = \frac{\hbar\omega}{k_B T}. \tag{4.5}$$

Using Eq. (4.5) we can express Eq. (4.4) in unitless form. Differentiating Eq. (4.4) with respect to temperature results in the heat capacity, C_V which is also expressed in unitless from below.

$$U(z) = \frac{3Vk_B^4T^4}{2\pi^2\nu^3\hbar^3}\int_0^{z_D} dz\left(\frac{z^3}{e^z-1}\right) \tag{4.6}$$

$$C_V(z) = \frac{3Vk_B^4T^3}{2\pi^2\nu^3\hbar^3}\int_0^{z_d} dz\left(\frac{z^4e^z}{(e^z-1)^2}\right) \tag{4.7}$$

It is important to note the similarities in the forms of Eq. (4.6)-(4.7) to those of the ${}^nL(x)$. For the energy it is identical with a different coefficient. For the heat capacity an extra factor of e^z is present in the numerator while the usual denominator is squared. Finally, the energy and heat capacity can be divided by the volume, so the integrand defines the thermal energy density $u(z)$ per frequency increment, and the volumetric heat capacity $\kappa_V(z)$ (units of $J.m^{-3}.K^{-1}$) per frequency increment, both are found below. Through use of unitless variables, the Planck distribution, and comparison of analytical form, extension of the techniques proposed in this thesis into the realm of phonons is viable.

$$u(z) = \frac{3}{2\pi^2\nu^3\hbar^3}\left(\frac{z^3}{e^z-1}\right)(k_B\,T)^4 \tag{4.8}$$

$$\kappa_V(z) = \frac{3}{2\pi^2\nu^3\hbar^3}k_B\left(\frac{z^4e^z}{(e^z-1)^2}\right)(k_B\,T)^3 \tag{4.9}$$

Conclusion

The thesis has proposed a generalized form Eq. (2.4) of 18 PDFs representing Planck's thermal radiation law for three spectral variables, wavelength, frequency, and wave number. Solutions of eight pairs of transcendental equations solved using Newton's method, Tables 4, 5 and generalized forms of the transcendental equations, Eq. (2.5) - (2.6) are presented and discussed. Displacement laws are proposed for peak, and inflection point positions. Three unitless parameters, derived from the peak, left, and right inflection points are assessed and compared to traditional statistical parameters for: standard deviation of the thermal radiation (inflection point deviation), slope ratio inflection point and standard deviation slope ratio, and relative area bound by the inflection points and standard deviations. Application in Photobiology, based on the quantum properties of the photons, suggests Nature's preference of the photon and power radiance PDFs per unit wavelength, $L_{\lambda}^{ph}(v,T)$ for biological processes. Extensions for the heat capacity and thermal energy of phonons are suggested. Thus, the thesis suggests generalizations of the analytical form of Planck's thermal radiation law exhibit important properties useful across many fields.

Appendix A

Positions of the Characteristic Points and Newton's Numerical Method for Solving Equations

The focus of this appendix is to provide further information for the topics discussed in Chapter 2. The first is the full precision solutions to the transcendental equations (Eq. 2.5-2.6) found in Tables A.1, A.2. The second is discussion of Newton's method for finding the roots of equations.

Newton's method is a second order numerical method (error shrinks in powers of 2 per iteration) that takes the form of [12]

$$x_{k+1} = x_k - \frac{f(x_k)}{f'(x_k)}. \tag{A.1}$$

Where x_k is the numerical result of the kth iteration, $f(x_k)$ and $f'(x_k)$ is the chosen function, and its derivative evaluated at x_k. The method requires a function of the form $f(x) = 0$ that is continuous, locally differentiable, and has a well-behaved derivative about the root. The functions $f(x)$ used are the transcendental equations for the various forms of Planck's thermal radiation law. The transcendental equations are listed below for convenience.

$$(x - n)e^x + n = 0 \tag{2.5a}$$

$$(x^2 - 2nx + n(n-1)e^{2x} + \left(x^2 + 2nx - 2n(n-1)\right)e^x + n(n-1) = 0 \tag{2.5b}$$

$$(1 - n\tilde{x})e^{1/\tilde{x}} + n\tilde{x} = 0 \tag{2.6a}$$

$$(n(n+1)\tilde{x}^2 - 2(n+1)\tilde{x} + 1)e^{2/\tilde{x}} + (-2n(n+1)\tilde{x}^2 + 2(n+1)\tilde{x} + 1)e^{1/\tilde{x}} + n(n+1)\tilde{x}^2 = 0 \tag{2.6b}$$

Eq. (2.5)-(2.6) are of the form $f(x) = 0$, and are differentiable, satisfying the basic requirements for Newton's method. Differentiating and using Eq. (A.1) a general solution to each of the four transcendental equations is found. For Eq. (2.5) the forms of Newton's method are

$$x_{k+1} = x_k - \frac{(x_k - n)e^{x_k} + n}{(x_k - n + 1)e^{x_k}}, \tag{A.2a}$$

$$x_{k+1} = x_k - \frac{\left(x_k^2 - 2nx_k + n(n-1)\right)e^{2x_k} + \left(x_k^2 + 2nx_k - 2n(n-1)\right)e^{x_k} + n(n-1)}{\left(2x_k^2 - (4n-2)x_k + 2n(n-2)\right)e^{2x_k} + \left(x_k^2 + (2n+2)x_k - 2n(n-2)\right)e^{x_k}}. \tag{A.2b}$$

For Eq. (2.6) the forms of Newton's method are

$$\tilde{x}_{k+1} = \tilde{x}_k - \frac{(1-n\tilde{x})e^{\frac{1}{\tilde{x}_k}} + n\tilde{x}_k}{-(\tilde{x}_k^{-2} - n\tilde{x}_k^{-1} + n)e^{\frac{1}{\tilde{x}_k}}} \tag{A.3a}$$

$$\tilde{x}_{k+1} = \tilde{x}_k - \frac{(n(n+1)\tilde{x}_k^2 - 2(n+1)\tilde{x}_k + 1)e^{\frac{2}{\tilde{x}_k}} + (-2n(n+1)\tilde{x}_k^2 + 2(n+1)\tilde{x}_k + 1)e^{\frac{1}{\tilde{x}_k}} + n(n+1)\tilde{x}_k^2}{(2n(n+1)\tilde{x}_k - (2+2n)(n+1) + 4(n+1)\tilde{x}_k^{-1} - 2\tilde{x}_k^{-2})e^{\frac{2}{\tilde{x}_k}} + (-4n(n+1)\tilde{x}_k + (2+2n)(n+1) - 2(n+1)\tilde{x}_k^{-1} - \tilde{x}_k^{-2})e^{\frac{1}{\tilde{x}_k}} + 2n(n+1)\tilde{x}_k}. \tag{A.3b}$$

Consider the unitless PDF $\left(\frac{x^3}{e^x-1}\right)$, the peak position must be found with an error < 10^{-6}. The error can be defined as $|x_{peak} - x_k|$. However, this requires the exact solution to be known. Using that $f(x_{peak}) = 0$, the error can instead be defined as the error in y, $f(x_k)$. To find the peak position the power index and initial guess x_o must be used in Eq. (A.2a). The initial guess can be chosen by approximating a solution of Eq. (2.5a) for n=3, or by graphing the function and choosing a point near the solution. Using these methods, the solution lies between x=2 and x=3. Choosing $x_o = 2.5$ the first iteration of Eq. (A.2a) returns $x_1 = 3.00749$ our new guess of the solution. Repeating this process five times results in $x_6 = 2.8214394$, with a value $f(x_6) < 10^{-6}$ satisfying the criteria, see Table A.1 for value of $f(x_6)$. To find the inflections points the same procedure is conducted with Eq. (2.5b) and Eq. (A.2b). Choosing $x_o = 1$ yields $x_1 = 0.969448$, repeating three times yields $x_4 = 0.9662677$ with $f(x_4) < 10^{-6}$ for the left inflection point. Choosing $x_o = 5$ yields $x_1 = 4.7983593$, repeating three times yields $x_7 = 4.6232470885$ with $f(x_7) < 10^{-6}$ for the right inflection point, see Table A.2 for values of f. Using Eq. (A.3), the inflection points and peak positions can be calculated for ${}^nL(\tilde{x})$ PDFs.

Table A.1. Summary of the peak positions at full precision required for the transcendental equations, $f(u) < 10^{-6}$ where u is the same as in $^{n}L(u)$.

Unitless PDF	Peak Position f(x)<1ppm (Decimal Places)	Value of f(x) at Peak	Value at Peak for Rounded
$\left(\frac{x^2}{e^x-1}\right)$	1.593624 (6)	−7.5972065927×10−7	0.00110
$\left(\frac{\tilde{x}^2}{e^{\tilde{x}}-1}\right)$	0.6275003 (7)	8.727784695×10−7	-0.00232
$\left(\frac{x^3}{e^x-1}\right)$	2.8214394 (7)	3.8474365205×10−7	-0.00606
$\left(\frac{\tilde{x}^3}{e^{\tilde{x}}-1}\right)$	0.354429 (6)	8.9400439141×10−7	0.01677
$\left(\frac{x^4}{e^x-1}\right)$	3.9206904 (7)	2.3807882243×10−7	0.01438
$\left(\frac{\tilde{x}^4}{e^{\tilde{x}}-1}\right)$	0.25505712 (8)	−2.4515080854×10−8	0.01041
$\left(\frac{x^5}{e^{\tilde{x}}-1}\right)$	4.96511423 (8)	−2.4127688381×10−7	-0.01580
$\left(\frac{\tilde{x}^5}{e^{\tilde{x}}-1}\right)$	0.201405236 (9)	−4.9954864068×10−7	0.28117

Table A.2. Summary of the inflection point positions at full precision required for the transcendental equations, $f(u) < 10^{-6}$ where u is the same as in $^{n}L(u)$.

Function Type	IPL for f(u)<1ppm (Decimal Places)	IPR for f(u)<1ppm (Decimal Places)	Value at IPL	Value at IPR	Value at IPL for Rounded	Value at IPR for Rounded
$\left(\frac{x^2}{e^x-1}\right)$	0	3.08609377 (8)	0	3.3224762319×10−7	0	-0.0814
$\left(\frac{\tilde{x}^2}{e^{\tilde{x}}-1}\right)$	0.21629819497 (11)	1.03491 (5)	−9.7485807871×10−7	8.1741455915×10−7	9.4978	0.00049
$\left(\frac{x^3}{e^x-1}\right)$	0.9662677 (7)	4.6232470885 (10)	2.1324862409×10−7	−8.4121893451×10−8	0.0014	−7.7594
$\left(\frac{\tilde{x}^3}{e^{\tilde{x}}-1}\right)$	0.167744084196 (12)	0.5390829 (7)	−9.0291714294×10−7	−6.8511206441×10−7	-144.57	−0.0073
$\left(\frac{x^4}{e^x-1}\right)$	1.85500223 (8)	5.96146209747 (11)	6.3249308013×10−7	−2.6608904591×10−7	0.0002	310.12
$\left(\frac{\tilde{x}^4}{e^{\tilde{x}}-1}\right)$	0.1384610883083 (13)	0.370509632 (9)	−3.0082944563×10−7	−1.7716941958×10−7	4003.02	5.7163
$\left(\frac{x^5}{e^{\tilde{x}}-1}\right)$	2.698985163 (9)	7.2222457025156 (13)	−3.2137491246×10−7	−6.3471088652×10−7	-0.01102	-2027.01
$\left(\frac{\tilde{x}^5}{e^{\tilde{x}}-1}\right)$	0.11841972376673 (14)	0.2837572965 (10)	−3.1116880406×10−8	5.9160136523×10−7	47060	1.1914

Appendix B

Tables for the Characteristic Points

Chapter 3 refers to various graphs of data, while this provides a quick visualization of the data it lacks numerical depth. This section provides the numerical values shown in the figures for the reader to see.

Table B.1. The following parameters for ${}^{n}L(x)$; (i) relative position to the peak of the standard deviation, $|x_0 - x_{\pm i}|$ and $\sigma_{\pm}$, (ii) ratio of the relative positions, and (iii) width of the distribution, $x_{+i} - x_{-i}$ and $\sigma_+ + \sigma_-$. The parameters are split into inflection point and statistical parameters.

	Inflection Point Parameters				Statistical Parameters			
${}^{n}L(x)$	$x_0 - x_{-i}$	$x_{+i} - x_o$	$\frac{x_o - x_{-i}}{x_{+i} - x_o}$	$x_{+i} - x_{-i}$	σ_-	σ_+	$\frac{\sigma_-}{\sigma_+}$	$\sigma_+ + \sigma_-$
${}^{2}L(x)$	N/A*	**1.492**	N/A	N/A	0.944	**1.456**	0.648	2.4
${}^{3}L(x)$	1.855	**1.802**	1.03	3.66	1.301	**1.789**	0.727	3.09
${}^{4}L(x)$	2.065	**2.041**	1.01	4.1	1.551	**2.049**	0.757	3.6
${}^{5}L(x)$	2.266	**2.257**	1.00	4.52	1.775	**2.285**	0.777	4.06

*$x_{-i} = 0$

Table B.2. The following parameters for ${}^{n}L(\tilde{x})$,; (i) relative position to the peak of the standard deviation, $|\tilde{x}_0 - \tilde{x}_{\pm i}|$ and $\tilde{\sigma}_{\pm}$, (ii) ratio of the relative positions, and (iii) width of the distribution, $\tilde{x}_{+i} - \tilde{x}_{-i}$ and $\tilde{\sigma}_+ + \tilde{\sigma}_-$. The parameters are split into inflection point and statistical parameters.

	Inflection Point Parameters				Statistical Parameters			
${}^{n}L(\tilde{x})$	$\tilde{x}_o - \tilde{x}_{-i}$	$\tilde{x}_{+i} - \tilde{x}_o$	$\frac{\tilde{x}_o - \tilde{x}_{-i}}{\tilde{x}_{+i} - \tilde{x}_o}$	$\tilde{x}_{+i} - \tilde{x}_{-i}$	$\tilde{\sigma}_-$	$\tilde{\sigma}_+$	$\frac{\tilde{\sigma}_-}{\tilde{\sigma}_+}$	$\tilde{\sigma}_+ + \tilde{\sigma}_-$
${}^{2}L(\tilde{x})$	0.411	0.407	1.01	0.819	0.268	0.652	0.411	0.92
${}^{3}L(\tilde{x})$	0.187	0.185	1.01	0.371	0.094	0.166	0.566	0.26
${}^{4}L(\tilde{x})$	0.117	0.115	1.01	0.233	0.055	0.075	0.733	0.13
${}^{5}L(\tilde{x})$	0.083	0.082	1.01	0.166	0.031	0.039	0.795	0.07

Table B.3 The radiance at each characteristic point of ${}^{n}L(x)$, and ratios of the radiance between the points for T=5800 K.

${}^{n}L(x)$	Peak Radiance	IPL Radiance	IPR Radiance	IPL/IPR Radiance	IPL/Peak Radiance	IPR/Peak Radiance
${}^{2}L(x)$	0.211	0	0.149	0	0	0.704
${}^{3}L(x)$	0.232	0.090	0.160	0.565	0.390	0.690
${}^{4}L(x)$	7.586x10^7	3.485x10^7	5.177x10^7	0.673	0.459	0.683
${}^{5}L(x)$	1.682x10^8	8.196x10^7	1.139x10^8	0.719	0.487	0.677

Table B.4. The radiance at each characteristic point of ${}^{n}L(\tilde{x})$, and ratios of the radiance between the points for T=5800K.

${}^{n}L(\tilde{x})$	Peak Radiance	IPL Radiance	IPR Radiance	IPL/IPR Radiance	IPL/Peak Radiance	IPR/Peak Radiance
${}^{2}L(\tilde{x})$	0.211	0.069	0.187	0.368	0.326	0.885
${}^{3}L(\tilde{x})$	0.232	0.090	0.193	0.464	0.387	0.833
${}^{4}L(\tilde{x})$	7.586x10^7	3.121x10^7	6.065x10^7	0.515	0.411	0.800
${}^{5}L(\tilde{x})$	1.682x10^8	7.240x10^7	1.308x10^8	0.553	0.430	0.778

Table B.5. The slope at each IP of ${}^{n}L(x)$, and ratio of the slopes IPsL/IPsR for T=5800K

${}^{n}L(x)$	IPsL	IPsR	IPsL/IPsR
${}^{2}L(x)$	0.326	-0.059	5.49
${}^{3}L(x)$	0.135	-0.058	2.33
${}^{4}L(x)$	3.384x10^7	-1.720x10^7	1.97
${}^{5}L(x)$	6.396x10^7	-3.510x10^7	1.82

Table B.6. The slope at each IP of ${}^{n}L(\tilde{x})$, and ratio of the slopes IPsL/IPsR for T=5800K

${}^{n}L(\tilde{x})$	IPsL	IPsR	IPsL/IPsR
${}^{2}L(\tilde{x})$	0.853	-0.080	10.7
${}^{3}L(\tilde{x})$	1.584	-0.287	5.52
${}^{4}L(\tilde{x})$	7.354x10^8	-1.810x10^8	4.06
${}^{5}L(\tilde{x})$	2.133x10^9	-6.320x10^8	3.38

Table B.7. The ratio of the area bound by the curve and the area bound by the inflection points (central integral radiance) and the ratio of the area bound by the curve and the area bound by one standard deviation from the peak for both set of functions ${}^{n}L(x)$ and ${}^{n}L(\tilde{x})$.

	PDF (v)		PDF (λ)	
${}^{n}L(u)$	$\int_{x_{-i}}^{x_{+i}} L\,dx / \int_{0}^{\infty} L\,dx$	$\int_{\sigma_{-}}^{\sigma_{+}} L\,dx / \int_{0}^{\infty} L\,dx$	$\int_{\tilde{x}_{-i}}^{\tilde{x}_{+i}} \tilde{L}\,d\tilde{x} / \int_{0}^{\infty} \tilde{L}\,d\tilde{x}$	$\int_{\tilde{\sigma}_{-}}^{\tilde{\sigma}_{+}} L\,d\tilde{x} / \int_{0}^{\infty} L\,d\tilde{x}$
${}^{2}L(u)$	0.658	0.581	0.146	0.169
${}^{3}L(u)$	0.670	0.602	0.287	0.219
${}^{4}L(u)$	0.667	0.612	0.414	0.249
${}^{5}L(u)$	0.667	0.621	0.468	0.223

References

1. Schroeder, Daniel V. Introduction to Thermal Physics. Robin J. Heyden, 2000, pp. 288–296.
2. Michael Nauenberg; Max Planck and the birth of the quantum hypothesis. *Am. J. Phys.* 1 September 2016; 84 (9): 709–720. https://doi.org/10.1119/1.4955146
3. Helge Kragh; Photon: New light on an old name. *arXiv.* 1 January 2014; https://doi.org/10.48550/arXiv.1401.0293
4. Max Planck and Morton Masius, The Theory of Heat Radiation (Philadelphia, P. Blakiston's Son & Co, [c1914]), http://archive.org/details/theoryofheatradi00planrich.
5. Tobias Wegener, Different Formulations of Planck's Law. Physics in a Nutshell, 2014, https://www.physics-in-a-nutshell.com/article/24/different-formulations-of-plancks-law.
6. Fritzsche, Hellmut. "Wien's law". Encyclopedia Britannica, 24 Oct. 2016, https://www.britannica.com/science/Wiens-law. Accessed 4 April 2024.
7. Leo, William R. Techniques for Nuclear and Particle Physics Experiments. 1993. 2nd ed., Springer-Verlag Berlin Heidelberg, pp. 86–88, project-cms-rpc-endcap.web.cern.ch/rpc/Physics/Books/[Dr._William_R._Leo__(auth.)]_Techniques_for_Nuclear.pdf. Accessed 4 Apr. 2024.
8. Tae, Jake. "Dissecting the Gaussian Distribution." Jake Tae, 12 Dec. 2019, jaketae.github.io/study/gaussian-distribution. Accessed 4 Apr. 2024.
9. Masahiko Taniguchi and Jonathan S. Lindsey, "Database of Absorption and Fluorescence Spectra of >300 Common Compounds for Use in PhotochemCAD," Photochemistry and Photobiology 94, no. 2 (March 2018): 290–327, https://doi.org/10.1111/php.12860.
10. Clementson, Lesley; Wojtasiewicz, Bozena; Gunasekera, Rasanthi (2021): Cyanobacterial cultures - absorption spectra, phycocyanin and phycoerythrin concentration for selected cultures. v1. CSIRO. Data Collection.
11. Kittel, Charles. Introduction to Solid State Physics. 8th ed., Hoboken, Nj, Wiley, 2005, pp. 107–113.
12. Gilat, Amos, et al. Numerical Methods for Engineers and Scientists : An Introduction with Applications Using MATLAB® /c Amos Gilat, Vish Subramaniam. Hoboken, Wiley, Copyright, 2014, pp. 66–71.